Publ. Astron. Soc. Japan (2015) 67 (1), L1 (1–6)
doi: 10.1093/pasj/psu138
Advance Access Publication Date: 2014 December 30
Letter

Letter

Witness of gas infall and outflow in the young starburst dwarf galaxy NGC 5253

Rie E. Miura,[1,*] Daniel Espada,[1,2,3] Hajime Sugai,[4] Kouichiro Nakanishi,[1,2,3] and Akihiko Hirota[1,2]

[1]National Astronomical Observatory of Japan, 2-21-1 Osawa, Mitaka, Tokyo 181-8588, Japan
[2]Joint ALMA Observatory, Alonso de Cordova 3107, Vitacura 763-0355, Santiago de Chile
[3]Department of Astronomical Science, The Graduate University for Advanced Studies (Sokendai), 2-21-1 Osawa, Mitaka, Tokyo 181-0015, Japan
[4]Kavli Institute for the Physics and Mathematics of the Universe, Todai Institutes for Advanced Study, The University of Tokyo (Kavli IPMU, WPI), 5-1-5 Kashiwanoha, Kashiwa, Chiba 277-8583, Japan

*E-mail: rie.miura@nao.ac.jp

Received 2014 August 22; Accepted 2014 October 28

Abstract

We present ^{12}CO(2–1) observations towards the dwarf galaxy NGC 5253 using the Submillimeter Array. The data shows that a large amount of molecular gas is located in the central $\sim$200 pc starburst region, physically associated with two young super stellar clusters (SSCs). The molecular gas traced by ^{12}CO(2–1) is elongated along the minor axis (dust lane) of the galaxy and its kinematics suggest that there is an inflow of molecular gas to the direction of the central SSCs, as is also observed in H I gas at a larger scale. Due to their correlation in spatial and velocity domains, the central SSCs were likely formed from molecular gas in the nucleus. We compare the ^{12}CO(2–1) with available H_2 1–0 S(1) data, and show that while the relatively cold gas traced by ^{12}CO(2–1) is distributed around the central starburst region but also along the dust lane, the warm gas traced by H_2 1–0 S(1) is associated with the central H II region and other star-forming regions. Interestingly, a cavity in the H_2 1–0 S(1) emission is found to be spatially correlated with a Hα shell. This Hα shell may trace a bipolar outflow from the central SSCs and the H_2 1–0 S(1) gas, the gas shocked by the outflow encountering the surrounding quiescent gas. We calculate a molecular gas inflow rate of $\sim 2\,M_\odot\,\mathrm{yr}^{-1}$, a star formation rate of 0.3–0.5 $M_\odot\,\mathrm{yr}^{-1}$, and an ionized gas outflow being emitted from the SSCs with a rate of (5–25)$\times\,10^{-3}\,f\,M_\odot\,\mathrm{yr}^{-1}$, where f is a volume filling factor.

Key words: galaxies: individual (NGC 5253) — galaxies: starburst — ISM: jets and outflows

1 Introduction

The nearest ($d = 3.8$ Mpc: Sakai et al. 2004) young nuclear starburst, NGC 5253, is arguably the best laboratory for understanding the star formation process at the very early stage of a starburst (Martín-Hernández et al. 2005; Caldwell & Phillips 1989). NGC 5253 is a compact blue dwarf galaxy, hosting several young clusters with ages ranging between < 2.5 and 50 Myr (Calzetti et al. 1997)

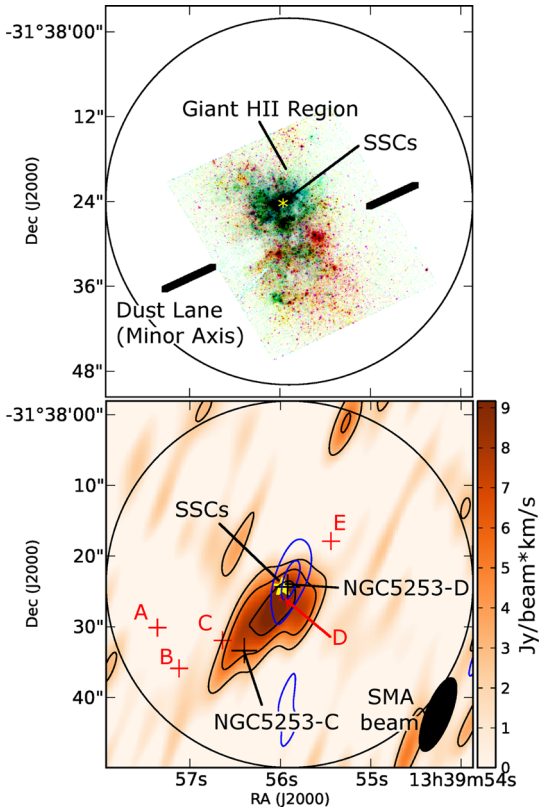

Fig. 1. Top: The three-color composite image of HST/ACS *F300W* (blue), *F658N* (Hα; green), and *F814W* (red) images. The locations of important regions discussed in this letter are denoted. The field of view of the SMA observations is shown as a circle. Bottom: The SMA CO(2–1) map of NGC 5253 in color scale and black contour. Black contour levels are 3σ, 6σ, and 9σ, where $1\sigma = 0.9$ Jy beam^{-1} km s^{-1}. The blue contours correspond to the 230 GHz continuum emission. Blue contour levels are 3 and 6σ, where $1\sigma = 3$ mJy beam^{-1}. The yellow star corresponds to the two massive and young SSCs. The black crosses are the two identified GMCs in this study. The red crosses are the five GMCs identified by M02. The synthesized beam size of the SMA observations is shown at the bottom right corner. (Color online)

and experiencing a few bursts in a short period (Davies et al. 1998). In the center of the galaxy, for which we assume $\alpha = 13^{\rm h}39^{\rm m}55\overset{\rm s}{.}7$ $\delta = -31^\circ38'24\overset{''}{.}4$ (J2000.0) following Turner and Beck (2004), there is a deeply embedded radio compact (1–2 pc size) H II region excited by 4700 O stars (Turner et al. 2000). It is powered by two massive ($\sim 3 \times 10^6\ M_\odot$) and young ($\sim 3.5$ Myr) super stellar clusters (SSCs) separated by $0\overset{''}{.}3$ (correponding to ~ 6 pc; Alonso-Herrero et al. 2004; Vanzi & Sauvage 2004).

The ionized gas around the central SSCs forms a giant H II region with multiple bubbles extending up to more than 100 pc (figure 1). The bubbles extend in the west–east direction from the central SSCs. The Hα line profiles of the bubbles are composed of three components: a broad component and two narrow components (Monreal-Ibero et al. 2010). Monreal-Ibero et al. (2010) interpreted that the broad and narrow components correspond to the outflow from the SSCs that expels the ambient gas and to the quiescent gas that the bipolar outflow has encountered, respectively. This scenario is also supported by the finding of diffuse X-ray components along the bipolar outflow (Summers et al. 2004). This implies that the Hα cone is filled with hot X-ray gas, as is also seen in starbursts such as NGC 253 (Boomsma et al. 2005; Strickland et al. 2002).

Just south of the central giant H II region and along the minor axis of the galaxy, there is a dust lane causing significant extinction in the optical image (see figure 1). The distribution of atomic gas (H I) is elongated along the dust lane, which is also the direction to M83 and other M83 subgroup members (Kobulnicky & Skillman 2008). The origin of the burst in NGC 5253 is believed to be due to infall of H I gas caused by the past interaction between this galaxy and the spiral galaxy M83 (Kobulnicky & Skillman 2008; López-Sánchez et al. 2012).

Several attempts have been made to detect CO transitions toward NGC 5253 to understand the properties of the molecular gas that fuel this starburst. Turner, Beck, and Hurt (1997) and Hirashita (2013) presented observations that resulted in marginal or no detections due to lack of sensitivity. Meier, Turner, and Beck (2002, hereafter M02) reported CO(2–1) emission detection along the dust lane using the Owens Valley Millimeter Array (OVRO), with resolutions of $10'' \times 5''$ (~ 177 pc $\times$ 88 pc). They suggested that the kinematics of the molecular gas support molecular gas inflow towards the center where the young SSCs are located.

In this letter, we present more sensitive new CO(2–1) and 230 GHz continuum observations obtained with the Submillimeter Array (SMA)[1] toward NGC 5253. We discuss the molecular gas inflow motion and calculate star formation rate (SFR) based on the continuum image. We also compare these data with other wavelength data to discuss the properties of gas outflow from the SSCs using available HST Hα and H_2 1–0 S(1) data (Davies et al. 1998).

2 Observations

^{12}CO(2–1) and 230 GHz continuum observations were performed towards NGC 5253 in 2009 September using the SMA for an observation time of two hours, as part of the legacy project B0DEGA (Espada et al. 2010). The full width at half maximum of the primary beam of SMA at 230 GHz is $52''$ (~ 1 kpc at the distance of 3.8 Mpc), which is enough to cover in a single pointing the nuclear region and also the dust lane.

[1] The SMA is a joint project between the Smithsonian Astrophysical Observatory and the Academia Sinica Institute of Astronomy and Astrophysics, and is funded by the Smithsonian Institution and the Academia Sinica.

The SMA data was reduced using the software package MIR-IDL,[2] and imaged using Miriad (Sault et al. 1995). Imaging was made with natural weighting. The resulting synthesized beam of the ^{12}CO images is $11'' \times 4''$, elongated due to the low elevation of the source at the SMA site. The final data cube and continuum data have a typical noise level of 0.03 Jy beam^{-1} at a velocity resolution of 20 km s^{-1} (corresponding to 15 MHz) with a number of channels of 25, and 3 mJy beam^{-1}, respectively. The sensitivity of our data (80 mJy beam^{-1} at 5 km s^{-1} resolution) is better than that of M02 (100 mJy beam^{-1} at 5 km s^{-1}), while the resolution is similar to theirs ($10'' \times 5''$). The continuum emission data was obtained from the line-free channels in the upper sideband. The effective bandwidth of line-free channels is 1.9 GHz. The ^{13}CO(2–1) and C^{18}O(2–1) emission lines were observed simultaneously in the lower sideband, but they were not detected in the data.

We compare the recovered total flux in the SMA interferometric observations with that of single-dish CO(2–1) data (Meier et al. 2001). M02 have reported a single-dish integrated intensity of 2.58 K km s^{-1}, corresponding to 98.65 Jy km s^{-1} for the 30″ beam of CSO at 230 GHz, which was measured pointing at $\alpha = 13^{\rm h}39^{\rm m}56\overset{\rm s}{.}6$ $\delta = -31^\circ 38' 30\overset{''}{.}2$ (J2000.0). The total flux measured over the single-dish beam is 27.6 Jy km s^{-1}, which suggests that $\sim$3/4 of the CO emission is resolved out in our interferometer observations.

3 Results

3.1 CO(2–1)

The CO(2–1) integrated intensity image in the velocity range of 330–430 km s^{-1} is shown in figure 1. The CO(2–1) emission peaks at the north of the dust lane and is elongated along the dust lane of the galaxy. We identified two GMCs with CLUMPFIND (Williams et al. 1994), hereafter called NGC5253-C and NGC5253-D, following the nomenclature in M02. Their positions and the physical parameters derived by using CLUMPFIND are given in figure 1 and table 1. These components are not resolved and thus the net size is expected to be smaller than the synthesized beam size. NGC5253-D is the most massive GMC and is found very close to the center, while NGC5253-C is less massive and located in the dust lane, to the south-east of the center.

The previous OVRO CO(2–1) map by M02 looks partially different from ours. The three GMCs (labeled as A, B, and E in figure 1) were also detected in M02. Since GMC B is located close to GMC C (with a separation of 9.″8 and 2 km s^{-1} in velocity), it is possibly blended with NGC5253-C in the SMA data. However, the two other GMCs (A and E) are not present in the SMA data, even though their intensities were larger than those of NGC5253-C/D, and the sensitivity of our data is better. These components may arise because they are located at the edge of their field-of-view and primary beam correction was applied. Note that because these two GMCs are compact, this difference cannot be due to missing flux.

The molecular gas mass is given by $M_{\rm mol} = 5.74 \times 10^4\, X_{\rm CO}^{\rm N5253} d_{\rm Mpc}^2 S_{\rm CO} R_{21/10}{}^{-1}\, (M_\odot)$, where $X_{\rm CO}^{\rm N5253}$ is the CO to H_2 conversion factor in 10^{20} cm^{-2} (K km s^{-1})$^{-1}$, $d_{\rm Mpc}$ is the distance to NGC 5253 in Mpc, $S_{\rm CO}$ is the CO(2–1) integrated flux density in Jy km s^{-1}, and $R_{21/10}$ is the CO(2–1)/CO(1–0) line ratio. Note that we do not include the helium abundance in the calculation. We use the same parameters as applied in M02 for the distance and the CO ratio, $d_{\rm Mpc} = 3.8$ and $R_{21/10}$ of unity (Meier et al. 2001), respectively. However, we use a different conversion factor because for metal-poor environments such as in this galaxy it is expected to be higher than the Galactic standard value (e.g., Leroy et al. 2011). We apply a conversion factor of $X_{\rm CO}^{\rm N5253} = 20$, corresponding to the metallicity of $12 + \log({\rm O/H}) = 8.16$ found for NGC 5253 (Kobulnicky et al. 1997), using the conversion factor versus metallicity relation in Leroy et al. (2011).

The derived molecular masses for the two GMCs are given in table 1. The mass of NGC5253-D is 74% of the total molecular gas mass recovered by SMA observations. Taking into account the velocity of the central SSCs ($V_{\rm lsr,\,SSC} = 390$ km s^{-1}: Schwartz & Martin 2004), NGC5253-D correlates well with the central SSCs not only spatially but also kinematically, implying a direct association between the GMC and the SSCs as well as the surrounding H II region. Thus NGC5253-D is likely the main gas reservoir feeding the current starburst.

To infer the distribution of molecular gas along the line of sight, we compare the spatial distribution between CO emission and the optical extinction. We present the CO velocity-separated map around $V_{\rm lsr,\,SSC}$ overlaid on the HST V-band image in figure 2. The blue and red contours represent the approaching and receding velocity components with respect to $V_{\rm lsr,\,SSC}$. The receding component is elongated along the dust lane and traces well the extinction in the optical image, which suggests that it is in front of the SSCs. The blue-shifted component is concentrated toward the SSCs and central giant H II region rather than the dust lane. The extinction does not match the blue-shifted component, which suggests that this component is likely located behind the central region. The CO gas kinematics and distribution in comparison with the dust extinction support a scenario in which the gas is falling into the central

[2] MIR is a software package to reduce SMA data based on the package originally developed by Nick Scoville at Caltech. See (http://cfa-www.harvard.edu/~cqi/mircook.html).

Table 1. GMC properties in NGC 5253.*

GMC	Positions†	$V_{\rm lsr}$ (km s^{-1})	$D_{\rm FWHM}$‡ (pc)	$V_{\rm FWHM}$‡ (km s^{-1})	$S_{\rm CO}$ (Jy km s^{-1})	$M_{\rm mol}$ ($10^6\,M_\odot$)	$M_{\rm vir}$ ($10^6\,M_\odot$)
NGC5253-C	+7.20, −9.30	420	105 × 97	6	3.8	3.2	1.2
NGC5253-D	0.00, −0.30	380	76 × 97	32	10.9	9.1	9.0

*Approximate errors are $\delta V_{\rm FWHM} = 10$ km s^{-1} (i.e., one-half the velocity resolution), $\delta M_{\rm mol} = 40\%$, $\delta M_{\rm vir} = 40\%$.
†Positions are offset from $\alpha = 13^{\rm h}39^{\rm m}55\overset{\rm s}{.}9$ $\delta = -31^\circ38'24\overset{''}{.}0$ in arcseconds.
‡The GMC sizes and velocity width are defined as the deconvolved FWHM diameters and the deconvolved FWHM velocity dispersion corrected for the beam size ($11'' \times 4''$) and velocity resolution (20 km s^{-1}) according to Williams, de Geus, and Blitz (1994).

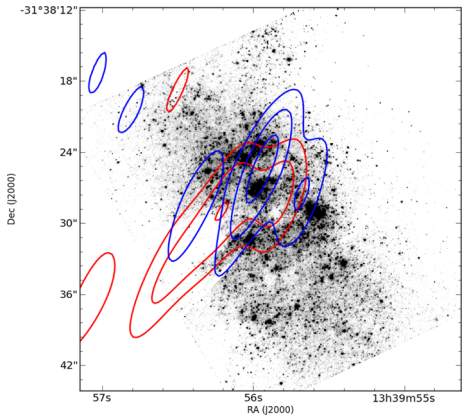

Fig. 2. SMA CO(2–1) image overlaid on the HST *V*-band (*F550M*) image. The blue (red) contours represent the molecular gas at approaching (receding) velocities with respect to the velocity of the central SSCs (390 km s^{-1}; Schwartz & Martin 2004). The integrated velocity ranges are 350–390 km s^{-1} and 390–430 km s^{-1} for the approaching and receding velocity components, respectively. Blue and red contour levels are 3σ, 5σ, and 7σ, where $1\sigma = 0.8$ Jy beam^{-1} km s^{-1}. (Color online)

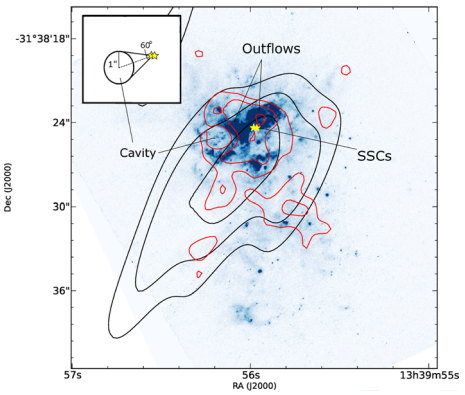

Fig. 3. CO(2–1) integrated intensity (black contour) and H_2 1–0 S(1) (red contour) maps overlaid on the HST Hα (*F658M*) image. Black contour levels are the same as in figure 1. Red contour levels are 1.7, 2.4, and 3.1×10^{-19} W m^{-2} arcsec^{-2}. The locations of the central two SSCs and the ionized gas outflow from the central SSCs are indicated on the map. A schematic view of the eastern outflow is indicated in the top left corner. (Color online)

starburst zone, as was suggested for the H I gas at a larger scale (Kobulnicky & Skillman 2008).

3.2 230 GHz continuum

The 230 GHz continuum emission was detected at $\alpha = 13^{\rm h}39^{\rm m}55\overset{\rm s}{.}9$ $\delta = -31^\circ38'23\overset{''}{.}3$, which is consistent with the position previously measured by M02 within the uncertainties. This position is practically coincident with that of the NGC5253-D component (offset only by $0\overset{''}{.}5$). The continuum component is not resolved. The net size is expected to be smaller than the synthesized beam size. The measured flux is 34 ± 9 mJy, also in agreement with M02 (46 ± 10 mJy) within the uncertainties.

The free–free emission from the gas ionized by OB stars contributes significantly to the emission at millimeter wavelengths and is optically thin. Other contributions to millimeter wavelength continuum emission, non-thermal radiation from SNRs and thermal emission from interstellar dust, are expected to be negligible at 230 GHz: the flux of synchrotron emission is very small shortward of 10 cm and no dust emission is detected at 1.3 mm (M02). Assuming that the 230 GHz continuum flux densities are entirely dominated by free–free emission from the ionized gas, we can calculate the total production rate of ionizing photons from the observed 230 GHz continuum flux densities. Equation (2) in Scoville et al. (1991) provides the relationship of the free–free emission flux density at 110 GHz to the total production rate of ionizing photons for optically thin plasma. Using a thermal (free–free) spectral index of −0.1, the relationship of the free–free emission flux density at 230 GHz (S_{230}) is given by: $S_{230} = (230/110)^{-0.1} \times 8.4 \times 10^{-2} \times Q^*_{49}/d^2_{\rm Mpc}$, where Q^*_{49} is the total production rate of ionizing photons in units of 10^{49} s^{-1}. The calculated total production rate of ionizing photons is $(6.3 \pm 1.7) \times 10^{52}$ s^{-1}.

3.3 Comparison with warm and ionized gas

In this subsection, we compare the morphology of CO with available H_2 1–0 S(1) (Davies et al. 1998) and archived HST Hα image (program no. 10608, PI: Vacca). All these data are displayed in figure 3. Although the distribution of CO

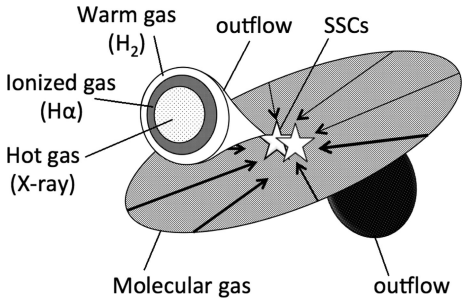

Fig. 4. Sketch view of the molecular gas disk traced by CO, the ionized gas traced by Hα, the shocked gas traced by H_2, and the hot gas traced by X-ray emission. The molecular gas around the central SSCs feeds the nucleus starburst region by gas inflow. The ionized gas forms a bipolar outflow from the central SSCs in NGC 5253, which is filled with hot X-ray gas, but the receding lobe suffers from high extinction due to dust and gas in front. The shocked gas is seen next to the ionized gas cone, which might be caused by the outflow encountering the ambient gas.

emission agrees well with that of H_2 1–0 S(1), the former is more extended along the dust lane. The peak of H_2 1–0 S(1) seems to be slightly offset from CO, and is at the central H II region. There is a cavity in H_2 1–0 S(1) emission at the east side of the SSCs which traces remarkably the shape of the Hα shell.

The CO(2–1) is emitted from gas at temperatures of ~ 16 K, while the H_2 1–0 S(1) emission traces heated gas by shocks (> 1000 K) or excited gas by UV radiation. The different distributions between CO(2–1) and H_2 1–0 S(1) suggest that while the cold molecular gas is more extended along the galaxy, the warm molecular gas is mostly distributed around the active star-forming regions. Besides, the warm molecular gas seems to be surrounding the cone of the ionized gas outflow from the SSC, which might have been caused by the shock where the energetic ionized outflow interacts with the ambient gas. Although Cresci et al. (2010) found that the dominant excitation mechanism of the H_2 emission does not seem to be shocks in NGC 5253, the shock mechanism may significantly contribute at least locally in this cavity structure.

4 Inflow and outflow from the super stellar clusters

We have shown that there is a signature of inflow motion in the relatively cold gas traced by CO. We have also found that the spatial correlation between H_2 1–0 S(1) and Hα emission supports the scenario suggested by Monreal-Ibero et al. (2010), in which the Hα emission traces the bipolar outflow from the central SSCs. In addition, diffuse X-ray emission is distributed similarly to the Hα emission, which suggests that it likely traces the hot gas outflow inside the Hα cone (Summers et al. 2004; see also figure 4) as observed in other starburst galaxies such as NGC 253 (Strickland et al. 2000). In this section, we calculate the balance of such inflow, outflow mass rates, and compare with the SFR assuming that NGC5253-D is the source feeding the formation of the central SSCs.

The gas inflow rate into the center of the galaxy can be calculated assuming that the radial inflow speed around the SSCs is ~ 20 km s^{-1}, corresponding to the radial velocity difference of the two components from the central SSCs (see figure 2). If we assume that the approximated distance from the inflowing molecular gas to the center of the galaxy is similar to the extent of the molecular gas of NGC5253-D, ~ 100 pc, and the amount of the molecular gas presumably associated with the SSCs is the NGC5253-D mass, $9.1 \times 10^6\ M_\odot$, then the gas inflow rate is estimated to be $1.9\ M_\odot\ \mathrm{yr}^{-1}$. This is in good agreement with the inflow gas rate derived from the H I data (Lelli et al. 2014).

Next we calculate the SFR using the measured stellar mass of NGC 5253 from the continuum emission (subsection 3.2). We calculate the total number of stars from the total ionizing photon rates using typical ionizing rates of O-type stars (09.5V–O3V: Martins et al. 2005), following the method described in Miura et al. (2010). O-type stellar spectral types are considered to be largely responsible for the ionizing photons of interstellar matter. We further assume that this region is characterized by a Salpeter initial mass function of 2.35 with mass limits of 0.1–58 $M_\odot$ (corresponding up to spectral type O3V). The total stellar mass is then estimated to be $5.3 \times 10^6\ M_\odot$. If half the total ionizing photons originate in the SSCs (M02), then the total stellar mass of the central SSCs is $\sim 10^6\ M_\odot$. This is consistent with the summation of the previously obtained masses of the two SSCs: one SSC has a mass of $5 \times 10^5\ M_\odot$, while the other has $(0.77\text{–}2.6) \times 10^6\ M_\odot$ (with the mass cutoffs of 1–100 $M_\odot$: Alonso-Herrero et al. 2004).

Since the central SSCs have been formed in < 2.5–4 Myr, the SFR for the the central starburst region is likely within 0.3–0.5 $M_\odot\ \mathrm{yr}^{-1}$. This is in good agreement with the previously obtained value from Hα flux densities ($0.270\ M_\odot\ \mathrm{yr}^{-1}$: Calzetti et al. 2004). The total stellar mass can also be compared with the mass of the molecular clouds to measure the star formation efficiency (SFE). The SFE is defined as $\mathrm{SFE} = M_{\mathrm{cl}}/(M_{\mathrm{cl}} + M_{\mathrm{mol}})$, where M_{cl} is the total stellar mass and M_{mol} is the molecular cloud mass. Taking into account that NGC5253-D is the parent GMC of the central SSCs, the SFE is estimated to be 10% using the half the total ionizing photons which might be originated from the central SSCs, while 37% using the total continuum flux density.

There is also outflow from the SSCs as can be witnessed in the H_2 1–0 S(1) and Hα images. We now estimate the mass-outflow rate of the ionized gas across a circular

cross section along the eastern bipolar outflow, which has a radius of 1″ for a cone opening angle of 60° [obtained directly from the size of the cavity in the H_2 1–0 S(1) and Hα emission; see figure 3], corresponding to a transverse area of the outflow of $A \sim 3.1 \times 10^{39}$ cm^2. The ionized gas outflow rate can be obtained from $\dot{M}_{\rm out} = 2 m_{\rm p} N_{\rm e} v_{\rm out} f A$ (Storchi-Bergmann et al. 2010), where the factor 2 is included to account for both sides of the outflow, $m_{\rm p}$ is the proton mass, $N_{\rm e}$ is the electron density, $v_{\rm out}$ is the velocity of the outflowing gas, and f is the filling factor. Assuming $N_{\rm e} = 458$–$2503\,{\rm cm}^{-3}$ (Guseva et al. 2011) and $v_{\rm out} = 70\,{\rm km\,s}^{-1}$ (an inclination of the outflow axis of 45° is assumed: Westmoquette et al. 2013), we obtain $\dot{M}_{\rm out} = (0.46\text{–}2.5) \times 10^{-2} f (v_{\rm out}/70\,{\rm km\,s}^{-1})\,[M_\odot\,{\rm yr}^{-1}]$. Thus the outflow rate is a small portion (0.2%–1.3%) of the gas inflow rate if the filling factor is assumed to be typically 0.01. Even taking into account that the mass injection rate is $\sim 0.2\,M_\odot\,{\rm yr}^{-1}$ (Summers et al. 2004), which is an upper limit because this was estimated from the total diffuse X-ray emission over the entire galaxy, the supplied molecular gas is larger than the total mass rate of the SFR and outflow masses.

We compare with the other starburst galaxy NGC 253 where outflows from the nucleus have been observed in X-ray, Hα, and CO molecular line emission (Strickland et al. 2000; Bolatto et al. 2013). The size, gas content, and star formation activity of this galaxy is much larger than that of NGC 5253.

NGC 253 has formed several SSCs in its nucleus, including a highly obscured SSC with mass of $1.4^{+0.4}_{-0.5} \times 10^7\,M_\odot$ (Kornei & McCrady 2009), which is about 10 times the SSC masses in NGC 5253. According to Strickland et al. (2000), a mass loss rate due to bipolar outflow cones of $0.7\text{–}1.3\,M_\odot\,{\rm yr}^{-1}$ is derived from X-ray and Hα data. The molecular gas outflow rate is $3\text{–}9\,M_\odot\,{\rm yr}^{-1}$, and such a large molecular gas outflow rate may lead to the termination of the starburst (Bolatto et al. 2013). With our NGC 5253 CO(2–1) data, it is difficult to distinguish a possible molecular gas outflow, even if it exists. Since the SSC masses, SFR, Hα, and X-ray outflows in NGC 5253 are roughly one-tenth of those in NGC 253, and if we assume the molecular gas outflow is also the same ratio ($0.3\text{–}0.9\,M_\odot\,{\rm yr}^{-1}$), the inflow rate can be equal to the summation of the outflow and SFR. Higher resolution and more sensitive observations with the Atacama Large Millimeter Array (ALMA) are mandatory to confirm this scenario and understand the feedback from the starburst.

References

Alonso-Herrero, A., Takagi, T., Baker, A. J., Imanishi, M., & Scoville, N. Z. 2004, ApJ, 612, 222

Bolatto, A. D., et al. 2013, Nature, 499, 450

Boomsma, R., Oosterloo, T. A., Fraternali, F., van der Hulst, J. M., & Sancisi, R. 2005, A&A, 431, 65

Caldwell, N., & Phillips, M. M. 1989, ApJ, 338, 789

Calzetti, D., Harris, J., Gallagher, J. S., Smith, D. A., III, Conselice, C. J., Homeier, N., & Kewley, L. 2004, AJ, 127, 1405

Calzetti, D., Meurer, G. R., Bohlin, R. C., Garnett, D. R., Kinney, A. L., Leitherer, C., & Storchi-Bergmann, T. 1997, AJ, 114, 1834

Cresci, G., Vanzi, L., & Sauvage, M. 2005, A&A, 433, 447

Cresci, G., Vanzi, L., Sauvage, M., Santangelo, G., & van der Werf, P. 2010, A&A, 520, A82

Davies, R. I., Sugai, H., & Ward, M. J. 1998, MNRAS, 295, 43

Espada, D., et al. 2010, in Galaxies and their Masks, ed. D. L. Block et al. (New York: Springer), 97

Guseva, N. G., Izotov, Y. I., Stasińska, G., Fricke, K. J., Henkel, C., & Papaderos, P. 2011, A&A, 529, A149

Hirashita, H. 2013, MNRAS, 429, 3390

Kobulnicky, H. A., & Skillman, E. D. 2008, AJ, 135, 527

Kobulnicky, H. A., Skillman, E. D., Roy, J. R., Walsh, J. R., & Rosa, M. R. 1997, ApJ, 477, 679

Kornei, K. A., & McCrady, N. 2009, ApJ, 697, 1180

López-Sánchez, Á. R., Koribalski, B. S., van Eymeren, J., Esteban, C., Kirby, E., Jerjen, H., & Lonsdale, N. 2012, MNRAS, 419, 1051

Lelli, F., Verheijen, M., & Fraternali, F. 2014, A&A, 566, A71

Leroy, A. K., et al. 2011, ApJ, 737, 12

Martín-Hernández, N. L., Schaerer, D., & Sauvage, M. 2005, A&A, 429, 449

Martins, F., Schaerer, D., & Hillier, D. J. 2005, A&A, 436, 1049

Meier, D. S., Turner, J. L., & Beck, S. C. 2002, AJ, 124, 877 (M02)

Meier, D. S., Turner, J. L., Crosthwaite, L. P., & Beck, S. C. 2001, AJ, 121, 740

Miura, R., et al. 2010, ApJ, 724, 1120

Monreal-Ibero, A., Vílchez, J. M., Walsh, J. R., & Muñoz-Tuñón, C. 2010, A&A, 517, A27

Sakai, S., Ferrarese, L., Kennicutt, R. C. Jr., & Saha, A. 2004, ApJ, 608, 42

Sault, R. J., Teuben, P. J., & Wright, M. C. H. 1995, ASP Conf. Ser., 77, 433

Scoville, N. Z., Sargent, A. I., Sanders, D. B., & Soifer, B. T. 1991, ApJ, 366, L5

Schwartz, C. M., & Martin, C. L. 2004, ApJ, 610, 201

Storchi-Bergmann, T., Lopes, R. D. S., McGregor, P. J., Riffel, R. A., Beck, T., & Martini, P. 2010, MNRAS, 402, 819

Strickland, D. K., Heckman, T. M., Weaver, K. A., & Dahlem, M. 2000, AJ, 120, 2965

Strickland, D. K., Heckman, T. M., Weaver, K. A., Hoopes, C. G., & Dahlem, M. 2002, ApJ, 568, 689

Summers, L. K., Stevens, I. R., Strickland, D. K., & Heckman, T. M. 2004, MNRAS, 351, 1

Turner, J. L., & Beck, S. C. 2004, ApJ, 602, L85

Turner, J. L., Beck, S. C., & Ho, P. T. P. 2000, ApJ, 532, L109

Turner, J. L., Beck, S. C., & Hurt, R. L. 1997, ApJ, 474, L11

Vanzi, L., & Sauvage, M. 2004, A&A, 415, 509

Westmoquette, M. S., James, B., Monreal-Ibero, A., & Walsh, J. R. 2013, A&A, 550, A88

Williams, J. P., de Geus, E. J., & Blitz, L. 1994, ApJ, 428, 693